Chinese Chemical Letters 34 (2023) 107849

Contents lists available at ScienceDirect

Chinese Chemical Letters

journal homepage: www.elsevier.com/locate/cclet

Regiocontrolled Rh(III)-catalyzed C–C coupling/C–N cyclization mediated by distinctive 1,2-migratory insertion of *gem*–difluoromethylene allenes: Reaction development and mechanistic insight

Zhi Zhou[1,*], Kaifeng Chen[1], Yi Wang[1], Xiuhua Zhong, Shuang Lin, Hui Gao*, Wei Yi*

Guangzhou Municipal and Guangdong Provincial Key Laboratory of Molecular Target & Clinical Pharmacology, NMPA and State Key Laboratory of Respiratory Disease, School of Pharmaceutical Sciences and the Fifth Affiliated Hospital, Guangzhou Medical University, Guangzhou 511436, China

ARTICLE INFO

Article history:
Received 15 July 2022
Revised 16 September 2022
Accepted 22 September 2022
Available online 25 September 2022

Keywords:
Gem-difluoromethylene allenes
C-H functionalization
Regiocontrol
Rhodium(III) catalysis
DFT calculations

ABSTRACT

By developing *gem*–difluoromethylene allenes as viable partners, regiocontrolled Rh(III)-catalyzed redox-neutral C–C coupling/C–N cyclization has been realized to build the pyridin-2(1*H*)-one motifs with the embedment of a *Z*-configured monofluoroalkene functionality, in which either (hetero)aromatic or vinylic amides were found to be compatible. Integrated experimental and computational mechanistic studies revealed that a tandem regioselective allene 1,2-insertion/β-H elimination/hydrogen transfer/oxidative addition/cyclization/*cis*-β-F elimination involving an unconventional Rh(III)-Rh(I)-Rh(III) catalytic cycle accounts for the established transformation. Through further FMO analysis and IGMH maps, a non-covalent weak interaction network between the *gem*–difluoromethylene part and the OPiv moiety was rationally defined for the unconventional and specific regioselectivity control.

Due to their unique physiochemical properties and therapeutic efficacies in drug discovery and development [1–5], fluorine-containing motifs have drawn considerable attention from synthetic chemists over the past decade [6–10]. As a consequence, diversified electrophilic, nucleophilic or free-radical fluorination and fluoroalkylation reagents have been developed to address their synthesis through converting fluoride-free starting materials to fluorine-containing chemicals in a highly efficient manner [11–15]. However, these reactions usually proceed with specially pre-functionalized substrates and under harsh conditions, thus giving limited types of fluorinated products with relatively low step-/atom-economy and functional group (FG) tolerance. Besides, recently environmental enforcement has given a great challenge for both the supply chain and the future use of these developed fluorinated reagents since environmentally harmful raw materials, solvents and/or additives were often involved for their preparation and application [16–18]. These serious situations greatly hindered their application. Therefore, further exploration of new, general and environmentally benign fluorinated reagents/methodologies for building fluorine-containing motifs remains one of the hottest topics.

Taking advantages of the exceptional advantage of C–H functionalization strategy in terms of activity, selectivity, atom-/step-economy, substrate scope and functional group tolerance [19–28], more recently, several easily available fluorinated π-compounds including perfluoroalkenes [29–32], *gem*–difluoroalkenes [33–40], *gem*–difluoromethylene alkynes [41–45], monofluoroalkynes [46] and *gem*–difluorocyclopropenes [47,48] have been developed as versatile coupling partners (CPs) to address this issue *via* transition metal (TM)-catalyzed C–H functionalization (Scheme 1a). Indeed, such fluorinated π-coupling partners-involved C–H activation mode often lead to the incorporation of the fluorine fragment into the structural backbone of the product, thereby delivering the corresponding fluorine-containing motifs with improved structural diversity and FG tolerance. Despite these notable progresses made in the organic integration of TM-catalyzed C–H activation with fluorinated π-compound CPs towards their synthesis, all the protocols developed to date remain limited to fluorinated alkyne/alkene-mediated reactions. Given the significance of fluorine-containing core in nature, thus, there is an urgent need to further expand the new fluorinated CPs with innovative C–H activation reaction mode to construct fluorine-containing motifs for meeting their increasing demands.

* Corresponding authors.
E-mail addresses: zhouzhi@gzhmu.edu.cn (Z. Zhou), gaoh9@gzhmu.edu.cn (H. Gao), yiwei@gzhmu.edu.cn (W. Yi).
[1] These authors contributed equally to this work.

https://doi.org/10.1016/j.cclet.2022.107849
1001-8417/

Inspired by the above information, we turn our attention to the allene species since it features impressive reactivity and has been successfully documented in recent C–H activation reactions as a class of versatile synthons [49–52]. However, owing to the presence of two orthogonal double bonds in the allene moiety, the chemo- and regioselectivity control remains a challenging topic for allene-mediated C–H activation reactions (Scheme 1b) [53,54]. In general, the substituent bearing a big steric and/or strong electronic effect is needed to be introduced for realizing the desired control of the selectivity, which would overshadow their further derivatization [55–58]. In view that the use of difluorinated π-compounds often leads to specific migratory insertion driven by the unique fluorine effect in the stage of C–H activation/C–C coupling [40,59,60], we envisioned that a reasonable strategy for achieving the chemo-/regioselectivity control of the allene moiety might be recognized by introducing the proper difluorine-containing fragment into the allene scaffold. Taking all these into account, we decided to design a new *gem*–difluorine-containing allene species to coordinate the reaction characteristics of the allene moiety and the *gem*–difluorine-enabled fluorine effect for the chemo-/regioselectivity control. To the best of our knowledge, such an assumption involving *gem*–difluorine-functionalized allenes has not been revealed to date in the field of C–H activation. Herein, we would like to report the first use of *gem*–difluoromethylene allenes for the regiocontrolled assembly of isoquinolone and pyridinone derivatives bearing a biologically important monofluoroalkene side chain [5,61] at the 3-position with exclusive *Z*-selectivity *via* Rh(III)-catalyzed C–C coupling/C–N cyclization (Scheme 1c).

To test our hypothesis, we commenced our investigation by employing *N*-pivaloyloxybenzamide **1a** with *gem*–difluoromethylene allene **2a** as model substrates. Preliminary screening demonstrated that the desired C–H coupling occurred under the classic Cp*Rh(III) catalytic system, resulting in the formation of the interesting 3-fluoroalkenyl isoquinolone framework **3aa** (see Table S1 in Supporting information for details). To our surprise, this transformation featured an unconventional allene insertion mode (*via* 1,2 double bond insertion) in comparison with previously reported TM-catalyzed C–H functionalization reactions involving monosubstituted allenes (*via* 2,1 or 2,3 double bond insertion) [53,54]. The introduction of the *gem*–difluoromethylene fragment might account for this phenomenon, thereby giving a fruitful expansion for the reaction manifold of allene substrates. Encouraged by this finding, we were next intrigued to probe the optimal reaction conditions. Preliminary examination of different TM catalysts gave inferior results, and the brief screening of the solvent and additive revealed that $[Cp^*RhCl_2]_2$/KOPiv in TFE was the optimal composition, affording **3aa** in 75% yield. The switch of other amide substrates bearing different oxidizing directing groups (ODGs) gave relatively low efficiency. After systematically screening of other experimental parameters such as catalyst loading, the reaction temperature and the ratio of starting materials, to the end, we were pleased to identify the optimized reaction conditions and furnished the desired product **3aa** in 81% isolated yield.

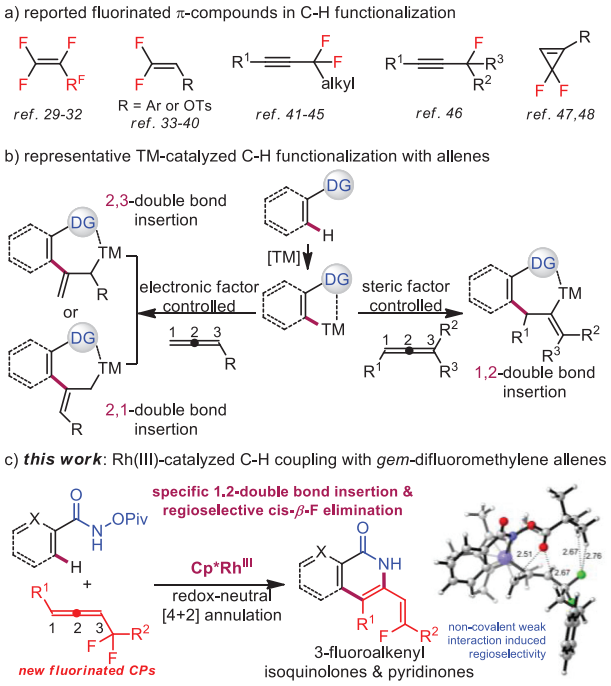

Scheme 1. TM-catalyzed C–H functionalization with fluorinated π-compounds.

Having established the optimal reaction conditions, we next explored the compatibility and generality of the developed protocol. As shown in Scheme 2a, a diverse array of *N*-pivaloyloxybenzamides were first examined to couple with *gem*–difluoromethylene allene **2a** and showed good FG tolerance. Various commonly encountered substituents including alkyl (**3ba** and **3ca**), methoxyl (**3da**), methylthio (**3ea**), halogens (**3fa**-**3ha**), trifluoromethyl (**3ia**), ester (**3ja**), cyano (**3ka**), nitro (**3la**) and phenyl (**3ma**) group were all tolerable to afford the desired cyclization products in moderate to good yields. The structure of compound **3aa** was further confirmed by X-ray crystallography and revealed a specific (*Z*)-selective configuration of the fluoroalkenyl moiety (CCDC: 2126006). Notably, *ortho*-substituted substrates that have been proven to be inefficient in most C–H activation cases were also feasible to participate in this transformation, delivering the corresponding fluoroalkenyl tethered isoquinolones in synthetically useful yields (**3na**-**3pa**). With *meta*-substituted *N*-pivaloyloxybenzamides being the substrates, the desired C–C coupling/C–N cyclization occurred effectively with a preference at the less-hindered site (**3qa**-**3ta**). Gratefully, the coupling of *gem*–difluoromethylene allene **2a** with complex *N*-pivaloyloxybenzamides derived from pharmaceutical ingredients such as probenecid (anti-gout agent), roflumilast (PDE-4 inhibitor) and pleconaril analog (antiviral agent) took place smoothly to yield the desired isoquinolone derivatives **3ua**-**3wa** in decent isolated yields, demonstrating the synthetic potential of the developed protocol for late-stage C–H modification of bioactive molecules.

Given the distinctive regioselectivity and FG compatibility demonstrated in benzamide substrates, we were next intrigued to extend the developed protocol to heteroaromatic and vinylic *N*-pivaloyloxy amides (Scheme 2b). As predicted, *N*-(pivaloyloxy)furan-2-carboxamide and *N*-(pivaloyloxy)thiophene-2-carboxamide were proved to be feasible for this transformation, affording the desired pyridinone derivatives **4aa** and **4ba** in moderate yields. Vinylic *N*-pivaloyloxy amides were also available substrates, leading to the formation of desired C–C coupling/C–N cyclization products **4ca**-**4ea** effectively. Subsequent examination of different *gem*–difluoromethylene allenes was conducted to further probe the robustness of this transformation (Scheme 2c). Interestingly, the results revealed that several 1,3-disubtituted allenes were also available CPs, furnishing the corresponding products **3ab**-**3ad** in decent yield with identically specific regioselectivity demonstrated by monosubstituted allenes, revealing that the presence of *gem*–difluorine moiety played a crucial role for determining the chemo-/regioselectivity control. Moreover, *gem*–difluoromethylene allenes derived from bioactive natural products, *e.g.*, cyclamen aldehyde and citronellal, were also good reactants for the developed transformation, delivering the desired fluorinated isoquinolones **3ae** and **3af** in 66% and 73% yields, respectively.

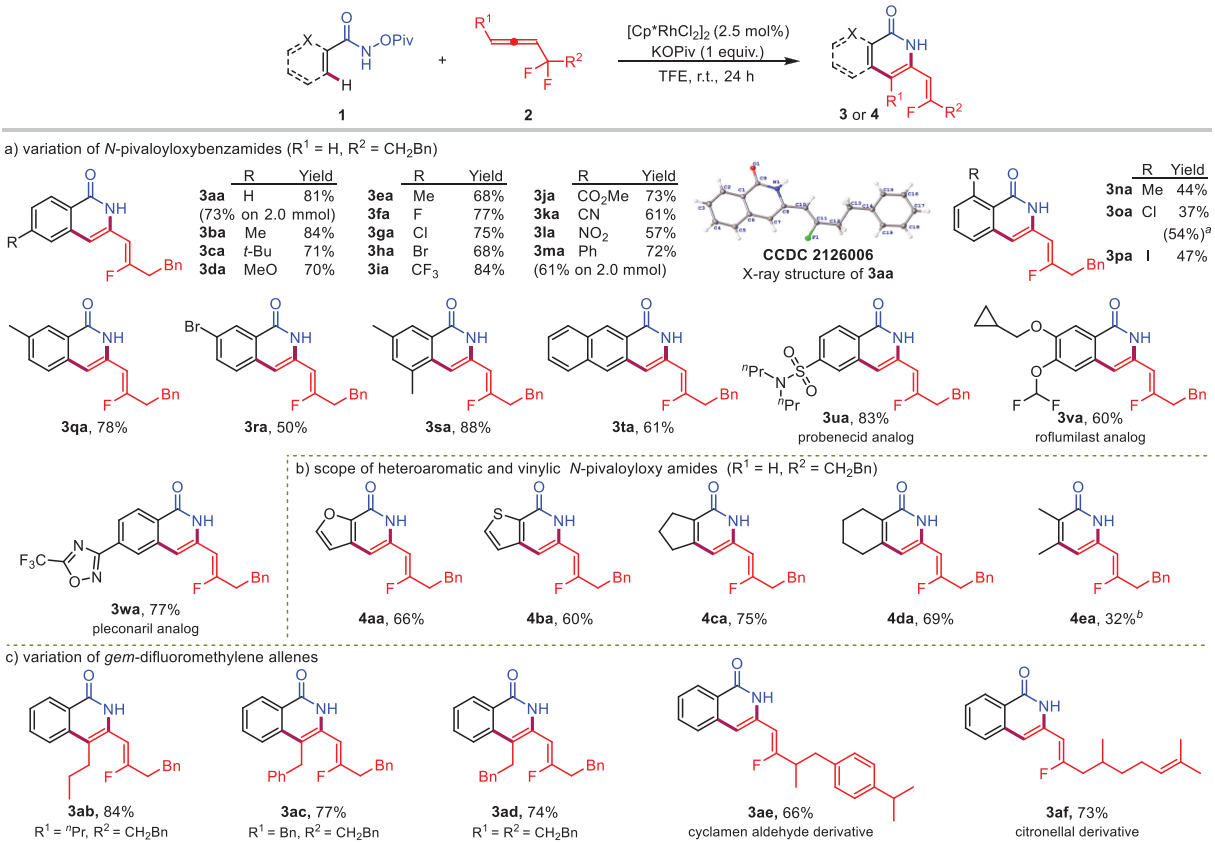

Scheme 2. Scope for (hetero)aromatic and vinylic C–H functionalization with *gem*–difluoromethylene allenes. Reaction conditions: **1** (0.2 mmol), **2** (0.2 mmol), $[Cp^*RhCl_2]_2$ (2.5 mol%) and KOPiv (1 equiv.) in TFE (0.1 mol/L) at room temperature for 24 h under air; isolated yields were reported. [a] The yield was obtained with 5 mol% of $[Cp^*RhCl_2]_2$ catalyst loading. [b] Dihydropyridin-2(1*H*)-one derivative **4ea'** was detected as the side-product, see Supporting information for details.

To further probe the reaction mechanism, in particular, to clarify the unconventional regioselectivity of the developed transformation, the detailed DFT calculations were next carried out using Gaussian 09 by selecting the five-membered rhodacycle **INT-1** as the starting point (zero value of energy) [37,62,63]. In consideration of the electron-withdrawing effect of the *gem*–difluoromethylene fragment, we envisioned that the allenic C–H bond cleavage might occur owing to its relatively high acidity. As shown in Fig. S1 (Supporting information), the coordination of *gem*–difluoromethylene allene to **INT-1** resulted in the formation of intermediate **INT-2a** with a free energy of −1.1 kcal/mol. Of note, the distinctive short distance of 2.16 Å between the allenic terminal hydrogen and the carbonyl oxygen of OPiv was observed in **INT-2a**, thus providing a possible allenic C–H bond activation step *via* concerted metalation deprotonation process. In this view, a Rh-assisted hydrogen transfer process probably occurred *via* **TS-1a** ($\Delta G^{\neq} = 29.4$ kcal/mol), affording the intermediate **INT-3a** with a free energy of 17.6 kcal/mol. The direct C–C bond reductive elimination from **INT-3a** was ruled out due to the relatively high energy barrier of 36.6 kcal/mol (from **INT-2a** to **TS-2a'**), while an alternative oxidative addition proceeded *via* **TS-2a** ($\Delta G^{\neq} = 26.8$ kcal/mol) to give the Rh(V) intermediate **INT-4a** along with the cleavage of N–O bond. Further C–C bond formation from **INT-4a** occurred facilely *via* **TS-3a** ($\Delta G^{\neq} = -2.7$ kcal/mol), delivering the key *ortho*-allenylation intermediate **INT-7b** with a free energy of −49.9 kcal/mol. To sum up, the unconventional allenic C–H bond activation process was involved with the overall energy barrier of 30.5 kcal/mol (from **INT-2a** to **TS-1a**).

Having clarified the unexpected allenic C–H bond activation process with a relatively high energy barrier, we were next intrigued to calculate the Gibbs energy profiles of other alternative reaction paths. Due to the equipment of two double bonds, classic double bond insertion was usually proposed for allene-involved C–H functionalization reactions. Herein we compared different insertion modes of the allene moiety into the C-Rh bond and the results were shown in Fig. 1. The coordination of 1,2-double bond in the *gem*–difluoromethylene allene to **INT-1** followed by the migratory insertion *via* **TS-1b** was more reasonable owing to the relatively low energy barrier of 15.1 kcal/mol (from **INT-2b** to **TS-1b**), delivering the seven-membered rhodacycle **INT-3b** with a free energy of −8.8 kcal/mol (Fig. 1A). As a comparison, other insertion modes involving contrary regioselectivity and different double bonds were ruled out since the high energy barriers of 17.1 (from **INT-2a** to **TS-1a'**), 19.2 (from **INT-1** to **TS-1b**) and 19.8 (from **INT-1** to **TS-1c**) kcal/mol were involved. These results were in line with the experimental observation that specific 1,2-regioselective allene insertion products were formed.

Moreover, the different regioselectivity for allene insertion was next illustrated by the calculated frontier molecular orbitals (Fig. 1B). The *gem*–difluoromethylene allene **2a** was selected as a model molecule, of which the HOMO-2 (−7.34 eV) and HOMO-3 (−7.58 eV) orbitals were closely related to the 1,2- and 2,3-double bond, respectively. Analyzing the HOMO and LUMO energies of the allene **2a** and the rhodacycle **INT-1**, it clearly revealed that the 1,2-double bond insertion was thermodynamically more favorable due to the relatively small HOMO-2/LUMO gap in comparison with 2,3-double bond insertion mode. To further clarify the difference between 1,2-/2,1-double bond insertion, and probe the potential role of the *gem*–difluoromethylene in controlling the observed regioselectivity, we then carried out detailed DFT calculations to in-

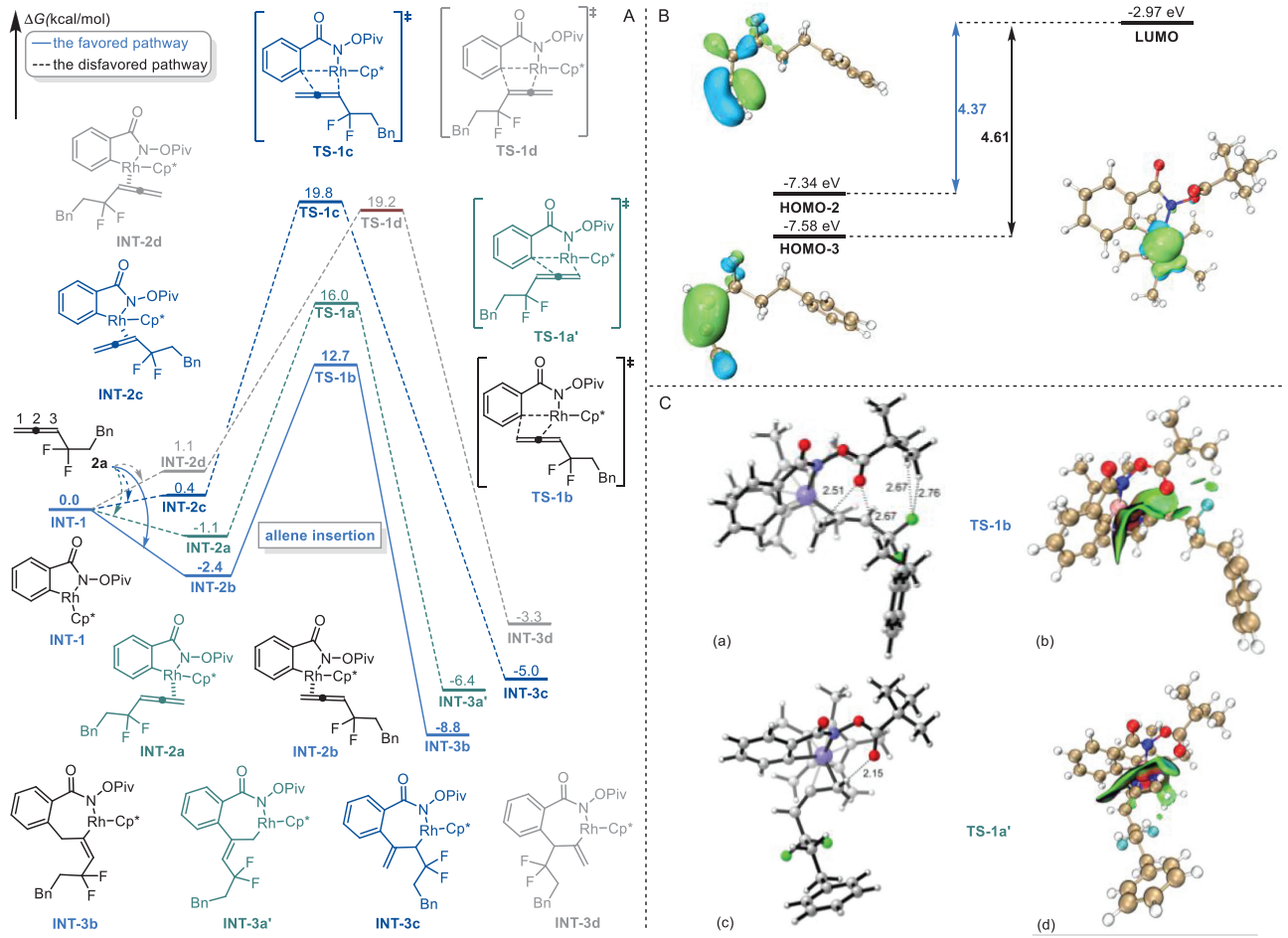

Fig. 1. Computational mechanistic studies for the allene insertion process. (A) Computed Gibbs energy profiles; (B) Calculated frontier-molecular-orbital (FMO) diagram for **2a** and **INT-1**, isovalue = 0.05; (C) Non-covalent interactions of **TS-1b**/**1a′**: Geometries of **TS-1b** (a), IGMH maps of **TS-1b** (b), Geometries of **TS-1a′** (c), IGMH maps of **TS-1a′** (d), isosurfaces of $\delta_g^{inter} = 0.004$ a.u.; green surfaces represent the weak interaction.

vestigate the non-covalent interactions of the transition states **TS-1b**/**1a′** [64]. As shown in Fig. 1C, both the carbonyl oxygen atom and the fluorine atom acted as hydrogen bond acceptors in **TS-1b** to form potent non-covalent weak interactions, thus rendering **TS-1b** in a relatively stable conformation. As a comparison, no obvious non-covalent interaction between the *gem*–difluoromethylene fragment and the rhodacycle species in **TS-1a′** was found, which probably accounted for the relatively high energy barrier of **TS-1a′** (17.1 *vs.* 15.1 kcal/mol).

With the mechanistic insight into a unique 1,2-double bond insertion established, the detailed reaction path for the formation of the final 3-fluoroalkenyl isoquinolone framework from intermediate **INT-3b** was then investigated (Fig. 2). Selective β-H elimination *via* **TS-2b** ($\Delta G^{\neq} = 2.8$ kcal/mol) afforded the allene intermediate **INT-5b** with a free energy of 1.2 kcal/mol, which further underwent a HOPiv-assisted hydrogen transfer *via* **TS-3b** ($\Delta G^{\neq} = 12.9$ kcal/mol) with an energy barrier of 21.7 kcal/mol (from **INT-3b** to **TS-3b**), delivering the Rh(I) species **INT-6b**. Subsequent oxidative addition *via* **TS-4b** ($\Delta G^{\neq} = 5.2$ kcal/mol) led to the cleavage of N–O bond, thus re-oxidizing the Rh(I) species to the Rh(III) intermediate **INT-7b** with an obvious exothermic process. By comparison, the highest energy barrier from **INT-1** to **INT-7b** involving the allene insertion process was 21.7 kcal/mol, which was obviously lower than that of the pathway shown in Fig. 1 (21.7 *vs.* 30.5 kcal/mol), suggesting that the allene insertion mode should be more reasonable than allenic C–H bond activation. Alternatively, other reaction pathways from **INT-3b** including sequential oxidative addition/β-H elimination *via* **TS-2b′** ($\Delta G^{\neq} = 1.0$ kcal/mol) and **TS-3b′** ($\Delta G^{\neq} = 17.4$ kcal/mol) and direct C–N reductive elimination *via* **TS-2b″** ($\Delta G^{\neq} = 15.4$ kcal/mol) were also excluded due to the high energy barriers of 32.6 (from **INT-4b′** to **TS-3b′**) and 24.2 (from **INT-3b** to **TS-2b″**) kcal/mol. Furthermore, the cyclization from **INT-7b** proceeded *via* the insertion of allene double bond into the N-Rh bond, affording the desired isoquinolone skeleton **INT-9b** *via* **TS-5b** ($\Delta G^{\neq} = -35.5$ kcal/mol). Finally, the selective β-F elimination was calculated and revealed that the product bearing a *Z*-type configuration was more favorable both thermodynamically (−91.2 *vs.* −89.2 kcal/mol) and dynamically (14.8 *vs.* 15.4 kcal/mol), which was in good agreement with our experimental results.

To gain more insight into the reaction mechanism, several experimental studies were further conducted. As shown in Scheme 3a, deuterium-labeling experiments in TFE-d_3 revealed that obvious deuterium incorporation was detected at the *ortho*-position of the ODG, suggesting a reversible C–H metalation process. In addition, the developed Rh(III)-catalyzed C–H coupling of *N*-pivaloyloxybenzamide **1a** with *gem*–difluoromethylene allene **2a** occurred smoothly in TFE-d_3 to give the desired product **3aa** without obvious deuteration at both the phenyl ring and the 3-fluoroalkenyl moiety, implying that the allene migratory insertion was fast and the fluoroalkenyl substituent was formed *via* β-F elimination rather than the protonolysis of C-Rh bond. Control experiments using allenic ketone **5** or monofluoroallene **7** as the CP were next conducted to define the role of the *gem*–difluoromethylene fragment. The results revealed that a mixture

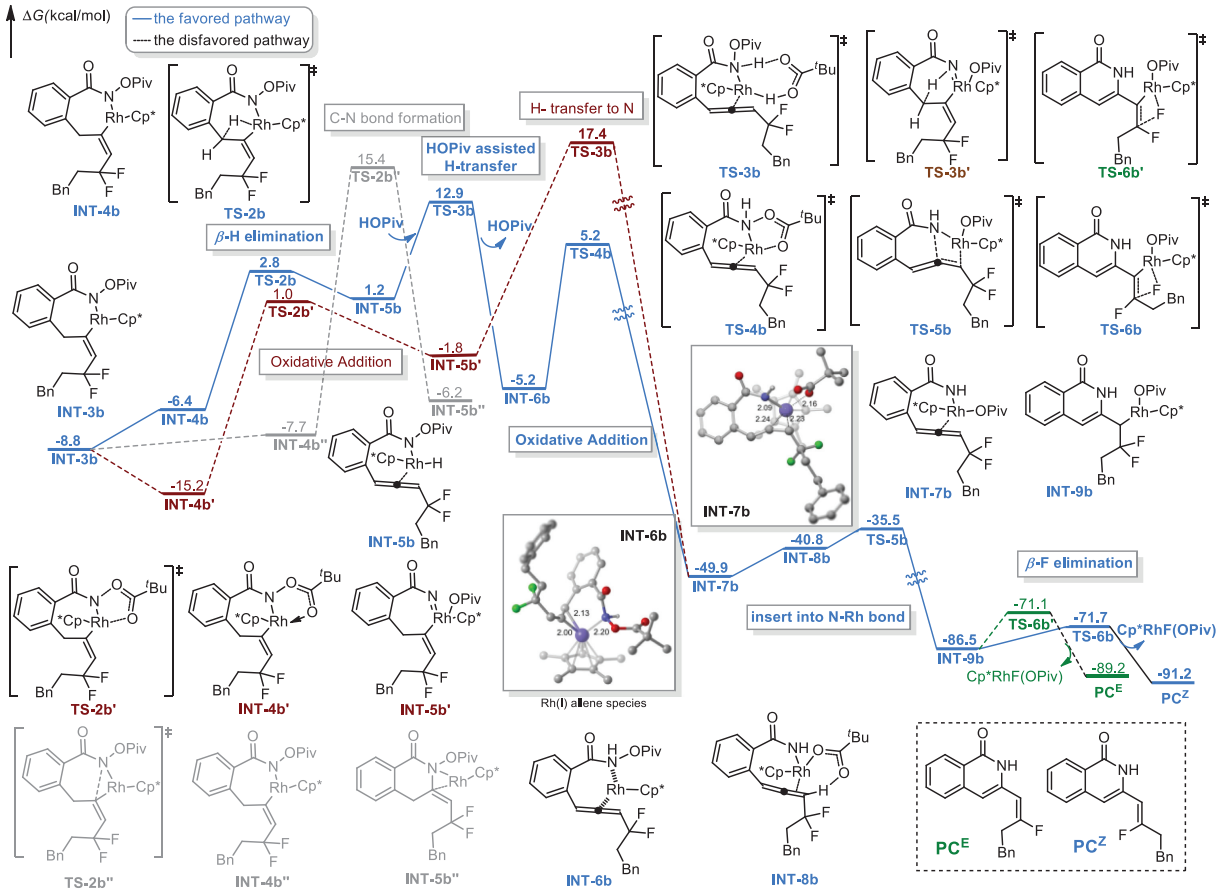

Fig. 2. Computed Gibbs free energy changes of the reaction pathway for the formation of 3-fluoroalkenyl isoquinolone from **INT-3b**.

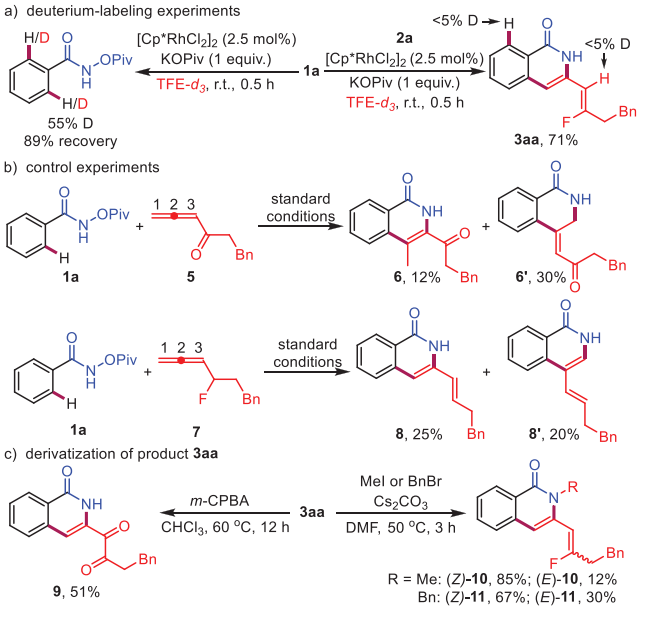

Scheme 3. Experimental mechanistic studies and product derivatization.

of regioisomers was obtained for both cases, illustrating that the equipment of the *gem*–difluoromethylene functionality in the allene substrate was crucial for realizing the specific regioselectivity (Scheme 3b). Further derivatization of product **3aa** was next carried out to probe the synthetic potential of this protocol (Scheme 3c). Exposure of **3aa** to *m*-CPBA led to the formation of dione derivative **9** *via* selective oxidation of the monofluorided alkene moiety, and the treatment of **3aa** with different halohydrocarbons delivered the *N*-substituted isoquinolones smoothly, albeit with a *Z*/*E* mixture. Taken together, these results further strengthen the synthetic potential of the developed protocol for the construction of intriguing isoquinolone frameworks.

On the basis of the above experimental and computational results, we proposed a HOPiv-assisted redox-neutral Rh(III)-Rh(I)-Rh(III) catalytic cycle involving a tandem regioselective allene 1,2-insertion/β-H elimination/hydrogen transfer/oxidative addition/cyclization/*cis*-β-F elimination sequence for the developed transformation [65–67] (Scheme 4). Initially, the active catalyst Cp*Rh(OPiv)$_2$ was formed readily *via* ligand exchange, followed by a reversible C–H metalation to afford the five-membered rhodacycle **A**. Subsequent regioselective migratory insertion of the allene 1,2-double bond into C-Rh bond delivered the intermediate **B** with an energy barrier of 15.1 kcal/mol, which underwent β-H elimination with an energy barrier of 11.6 kcal/mol to give the allene intermediate **C**. Sequential hydrogen transfer/oxidative addition process proceeded to furnish the intermediate **D**, which involved an energy barrier of 21.7 kcal/mol. Next, the intramolecular cyclization occurred *via* selective insertion of the allene double bond into the N-Rh bond with an energy barrier of 14.4 kcal/mol, and resulted in the construction of the isoquinolone framework. Finally, selective *cis*-β-F elimination to quench the C-Rh bond with an energy barrier of 14.8 kcal/mol led to the final formation of the product **3aa** and the active Rh(III) catalyst in a redox-neutral manner. The detailed DFT calculations demonstrated that the non-covalent weak interaction network between the *gem*–difluoromethylene part and the OPiv moiety attributed to the unconventional and specific regioselectivity.

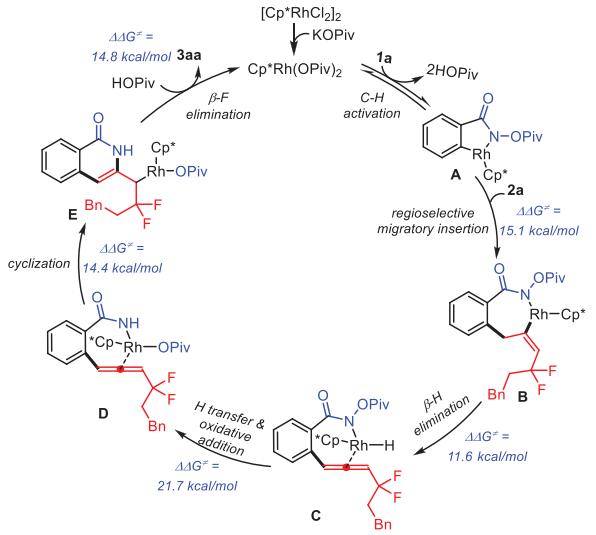

Scheme 4. Proposed catalytic cycle.

In conclusion, by virtue of newly-developed *gem*–difluoromethylene allenes as versatile CPs, an efficient and regiocontrolled Rh(III)-catalyzed C–H activation/C–C coupling/C–N cyclization cascade has been developed successfully for the construction of 3-fluoroalkenyl isoquinolones and pyridinones, in which a unique 1,2-migratory insertion of the allene unit was involved. Either (hetero)aromatic or vinylic amides with the embedment of various functional groups were proven to be viable substrates for the established transformation. Through combined DFT calculations and experimental mechanistic studies, the role of the *gem*–difluoromethylene moiety, the key function of the KOPiv additive as well as the origin of the chemo-/regioselectivity have been clarified accordingly. Further investigations on the scope and application of the innovative *gem*–difluoromethylene allene species in assembling othexr intriguing fluorine-containing motifs *via* TM-catalyzed C–H activation are in progress.

Declaration of competing interest

The authors declare that they have no known competing financial interests or personal relationships that could have appeared to influence the work reported in this paper.

Acknowledgments

We thank the National Natural Science Foundation of China (NSFC, Nos. 21877020, 22007020), Natural Science Foundation of Guangdong Province (No. 2019A1515010935) and Science and Technology Program of Guangzhou (No. 202102020615) for financial support on this study.

Supplementary materials

Supplementary material associated with this article can be found, in the online version, at doi:10.1016/j.cclet.2022.107849.

References

[1] J. Han, A.M. Remete, L.S. Dobson, et al., J. Fluorine Chem. 239 (2020) 109639.
[2] T. Liang, C.N. Neumann, T. Ritter, Angew. Chem. Int. Ed. 52 (2013) 8214–8264.
[3] Y. Zhou, J. Wang, Z. Gu, et al., Chem. Rev. 116 (2016) 422–518.
[4] E.P. Gillis, K.J. Eastman, M.D. Hill, D.J. Donnelly, N.A. Meanwell, J. Med. Chem. 58 (2015) 8315–8359.
[5] N.A. Meanwell, J. Med. Chem. 61 (2018) 5822–5880.
[6] P. Xiao, X. Pannecoucke, J.P. Bouillon, S. Couve-Bonnaire, Chem. Soc. Rev. 50 (2021) 6094–6151.
[7] M. Reichel, K. Karaghiosoff, Angew. Chem. Int. Ed. 59 (2020) 12268–12281.
[8] Y. Zhu, J.L. Han, J.D. Wang, et al., Chem. Rev. 118 (2018) 3887–3964.
[9] Q. Cheng, T. Ritter, Trends Chem. 1 (2019) 461–470.
[10] S. Hara, Stereoselective synthesis of mono-fluoroalkenes, in: J. Wang (Ed.), Stereoselective Synthesis of Mono-fluoroalkenes, Stereoselective Alkene Synthesis, Topics in Current Chemistry, vol. 327, Springer, Berlin, Heidelberg, 2012, pp. 59–86.
[11] Y.Y. See, M.T. Morales-Colon, D.C. Bland, M.S. Sanford, Acc. Chem. Res. 53 (2020) 2372–2383.
[12] M. Li, X.S. Xue, J.P. Cheng, Acc. Chem. Res. 53 (2020) 182–197.
[13] R. Szpera, D.F.J. Moseley, L.B. Smith, A.J. Sterling, V. Gouverneur, Angew. Chem. Int. Ed. 58 (2019) 14824–14848.
[14] Z. Feng, Y.L. Xiao, X. Zhang, Acc. Chem. Res. 51 (2018) 2264–2278.
[15] S. Barata-Vallejo, M.V. Cooke, A. Postigo, ACS Catal. 8 (2018) 7287–7307.
[16] J. Han, L. Kiss, H. Mei, et al., Chem. Rev. 121 (2021) 4678–4742.
[17] S. Caron, Org. Process Res. Dev. 24 (2020) 470–480.
[18] A. Harsanyi, G. Sandford, Green Chem. 17 (2015) 2081–2086.
[19] B. Zhao, B. Prabagar, Z. Shi, Chem 7 (2021) 2585–2634.
[20] R. Jana, H.M. Begama, E. Dinda, Chem. Commun. 57 (2021) 10842–10866.
[21] S. Shabani, Y.Z. Wu, H.G. Ryan, C.A. Hutton, Chem. Soc. Rev. 50 (2021) 9278–9343.
[22] L. Guillemard, N. Kaplaneris, L. Ackermann, M.J. Johansson, Nat. Rev. Chem. 5 (2021) 522–545.
[23] J. Zhang, X. Lu, C. Shen, et al., Chem. Soc. Rev. 50 (2021) 3263–3314.
[24] J. Wen, Z. Shi, Acc. Chem. Res. 54 (2021) 1723–1736.
[25] D. Sun, D.N. Confair, J.A. Ellman, Acc. Chem. Res. 54 (2021) 1766–1778.
[26] J. Mas-Roselló, A.G. Herraiz, B. Audic, A. Laverny, N. Cramer, Angew. Chem. Int. Ed. 60 (2021) 13198–13224.
[27] S.Y. Hong, Y. Hwang, M. Lee, S. Chang, Acc. Chem. Res. 54 (2021) 2683–2700.
[28] J. Huang, F. Liu, F. Du, L. Zeng, Z. Chen, Green Synth. Catal. (2022) https://doi.org/10.1016/j.gresc.2022.06.002.
[29] N. Li, Y. Wang, L. Kong, J. Chang, X. Li, Adv. Synth. Catal. 361 (2019) 3880–3885.
[30] D. Zell, U. Dhawa, V. Mueller, et al., ACS Catal. 7 (2017) 4209–4213.
[31] Y. Li, F. Xie, Y. Liu, X. Yang, X. Li, Org. Lett. 20 (2018) 437–440.
[32] B. Shu, S.Y. Chen, N.X. Deng, et al., Org. Chem. Front. 8 (2021) 4445–4451.
[33] P. Tian, C. Feng, T.P. Loh, Nat. Commun. 6 (2015) 7472.
[34] H.J. Tang, L.Z. Lin, C. Feng, T.P. Loh, Angew. Chem. Int. Ed. 56 (2017) 9872–9876.
[35] L. Kong, B. Liu, X. Zhou, F. Wang, X. Li, Chem. Commun. 53 (2017) 10326–10329.
[36] W.W. Ji, E. Lin, Q. Li, H. Wang, Chem. Commun. 53 (2017) 5665–5668.
[37] J.Q. Wu, S.S. Zhang, H. Gao, et al., J. Am. Chem. Soc. 139 (2017) 3537–3545.
[38] J. Hu, X. Han, Y. Yuan, Z. Shi, Angew. Chem. Int. Ed. 56 (2017) 13342–13346.
[39] J. Hu, Y. Zhao, Z. Shi, Nat. Catal. 1 (2018) 860–869.
[40] S. Koley, R.A. Altman, Isr. J. Chem. 60 (2020) 313–339.
[41] H. Gao, S. Lin, S. Zhang, et al., Angew. Chem. Int. Ed. 60 (2021) 1959–1966.
[42] Y. Yang, N. Li, J. Zhao, et al., Adv. Synth. Catal. 363 (2021) 3600–3606.
[43] T. Li, C. Zhou, X. Yan, J. Wang, Angew. Chem. Int. Ed. 57 (2018) 4048–4052.
[44] F. Romanov-Michailidis, B.D. Ravetz, D.W. Paley, T. Rovis, J. Am. Chem. Soc. 140 (2018) 5370–5374.
[45] C.Q. Wang, L. Ye, C. Feng, T.P. Loh, J. Am. Chem. Soc. 139 (2017) 1762–1765.
[46] X. Zhong, S. Lin, H. Gao, et al., Org. Lett. 23 (2021) 2285–2291.
[47] H. Xu, W. Chen, M. Bian, et al., ACS Catal. 11 (2021) 14694–14701.
[48] Y. He, L. Tian, X. Chang, et al., Chin. Chem. Lett. 33 (2022) 2987–2992.
[49] J.M. Alonso, P. Almendros, Chem. Rev. 121 (2021) 4193–4252.
[50] G. Li, X. Huo, X. Jiang, W. Zhang, Chem. Soc. Rev. 49 (2020) 2060–2118.
[51] X.L. Han, P.-P. Lin, Q. Li, Chin. Chem. Lett. 30 (2019) 1495–1502.
[52] J.L. Mascareñas, I. Varela, F. López, Acc. Chem. Res. 52 (2019) 465–479.
[53] B. Yang, Y. Qiu, J.E. Backvall, Acc. Chem. Res. 51 (2018) 1520–1531.
[54] J. Ye, S. Ma, Acc. Chem. Res. 47 (2014) 989–1000.
[55] R.K. Shukla, A.M. Nair, S. Khan, C.M.R. Volla, Angew. Chem. Int. Ed. 59 (2020) 17042–17048.
[56] S.-.G. Wang, Y. Liu, N. Cramer, Angew. Chem. Int. Ed. 58 (2019) 18136–18140.
[57] X. Vidal, J.L. Mascareñas, M. Gulías, J. Am. Chem. Soc. 141 (2019) 1862–1866.
[58] R. Zeng, S. Wu, C. Fu, S. Ma, J. Am. Chem. Soc. 135 (2013) 18284–18287.
[59] S. Liu, L. Zhu, T. Zhang, et al., Org. Lett. 23 (2021) 1489–1494.
[60] H. Wu, X. Li, X. Tang, C. Feng, G. Huang, J. Org. Chem. 83 (2018) 9220–9230.
[61] G. Landelle, M. Bergeron, M.O. Turcotte-Savard, J.F. Paquin, Chem. Soc. Rev. 40 (2011) 2867–2908.
[62] M. Bian, H. Mawjuda, H. Gao, et al., Org. Lett. 22 (2020) 9677–9682.
[63] S. Vásquez-Céspedes, X. Wang, F. Glorius, ACS Catal. 8 (2018) 242–257.
[64] T. Lu, Q. Chen, J. Comput. Chem. 43 (2022) 539.
[65] S. Rakshit, C. Grohmann, T. Besset, F. Glorius, J. Am. Chem. Soc. 133 (2011) 2350–2353.
[66] G. Liu, Y. Shen, Z. Zhou, X. Lu, Angew. Chem. Int. Ed. 52 (2013) 6033–6037.
[67] X.X. Ma, J.B. Liu, F. Huang, C.Z. Sun, D.Z. Chen, Catal. Sci. Technol. 8 (2018) 3590–3598.